LETTER

Parallel flow driven by electron cyclotron heating in the helically symmetric experiment

IOP Publishing | International Atomic Energy Agency Nuclear Fusion

Nucl. Fusion **62** (2022) 064004 (7pp) https://doi.org/10.1088/1741-4326/ac61bb

Letter

Parallel flow driven by electron cyclotron heating in the helically symmetric experiment

Y. Yamamoto[1,*,], S. Murakami[1], C.C. Chang[1], S.T.A. Kumar[2], J.N. Talmadge[2], K.M. Likin[2] and D.T. Anderson[2]**

[1] Department of Nuclear Engineering, Kyoto University, Kyoto 615-8540, Japan
[2] HSX Plasma Laboratory, University of Wisconsin-Madison, Madison, WI 53706, United States of America

E-mail: yamamoto.yasuhiro@qst.go.jp

Received 9 February 2022, revised 22 March 2022
Accepted for publication 28 March 2022
Published 19 April 2022

Abstract

Spontaneous plasma flows have been observed in electron cyclotron heating (ECH) plasmas in the helically symmetric experiment. A smaller parallel flow was observed in the quasi-helically symmetric configuration compared with that observed in the Mirror configuration, although the mirror configuration has a larger neoclassical viscosity. Using the GNET code, we evaluate the electromagnetic and collisional forces induced by ECH. We also evaluate the parallel flow driven by the ECH force, by solving the momentum balance equations and Ampère law. The obtained flows show reasonable agreement with results obtained from experiments. This work indicates that the radial electron current generated by ECH could drive the parallel flow.

Keywords: stellarator, plasma flow, parallel flow, ECH, $j \times B$ force, collisional force

(Some figures may appear in colour only in the online journal)

1. Introduction

Toroidal and poloidal flows have been found to play an important role in turbulence transport through sheared $E \times B$ flows [1, 2], as well as in magnetohydrodynamic instabilities such as the resistive wall mode [3–5]. Therefore, elucidating the mechanism of plasma flow generation is important work. Recently, spontaneous flows have been observed in electron cyclotron heating (ECH) plasmas in many tokamaks and helical devices such as the JT-60U, the large helical device and the helically symmetric experiment (HSX), even though ECH is not considered to act as a momentum source. To establish the underlying mechanism behind these observations, many experimental [6–11] and theoretical [12–14] studies have been undertaken. In this work, we indicate that ECH can induce the electromagnetic force and it acts as a momentum source in the HSX plasma.

The HSX is the first quasi-symmetric stellarator device, where two typical magnetic configurations are considered. One magnetic configuration used is the quasi-helically symmetric (QHS) configuration, which has quasi-helical symmetry in the magnetic field strength on the flux surface. It is dominated by the helical Fourier spectral component of the $(n = 4, m = 1)$ mode, where n and m are the toroidal and poloidal mode numbers, respectively. The second configuration considered is the mirror configuration; in this configuration a set of auxiliary coils adds the non-symmetric modes $(n = 4, m = 0)$ and $(n = 8, m = 0)$, which break the helical symmetry. Figure 1 shows the magnetic field spectrum of

* Author to whom any correspondence should be addressed.
** Present address: National Institutes for Quantum Science and Technology, Rokkasho, Aomori 039-3212, Japan.

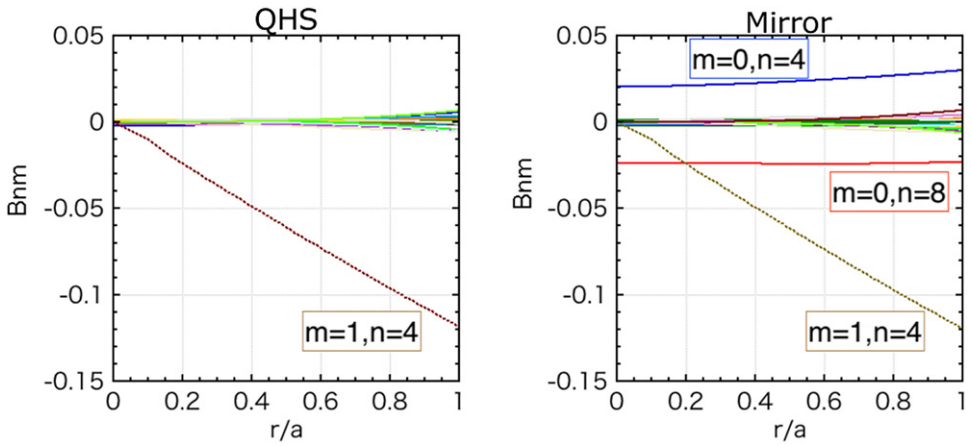

Figure 1. Magnetic field spectrum in the QHS configuration (left) and the mirror configuration (right).

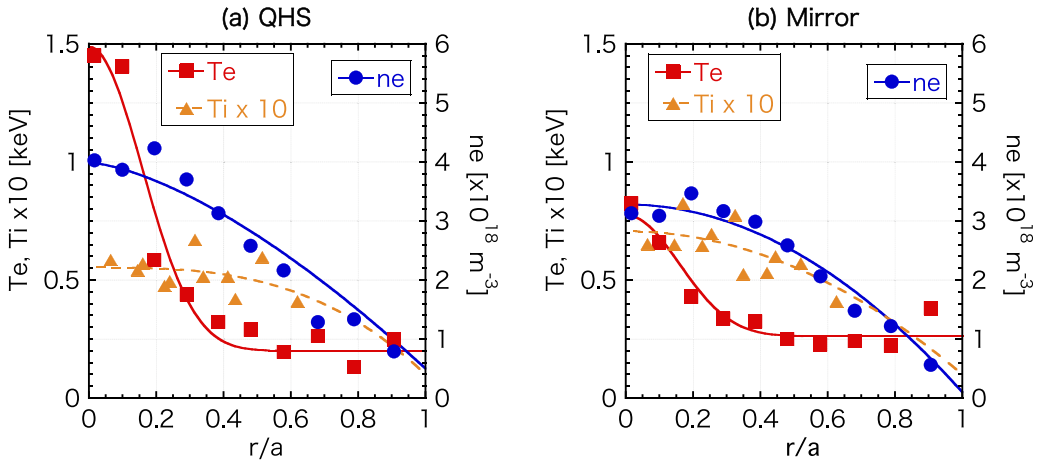

Figure 2. The radial temperature and density profiles of typical experiments in (*a*) the QHS and (*b*) mirror configurations.

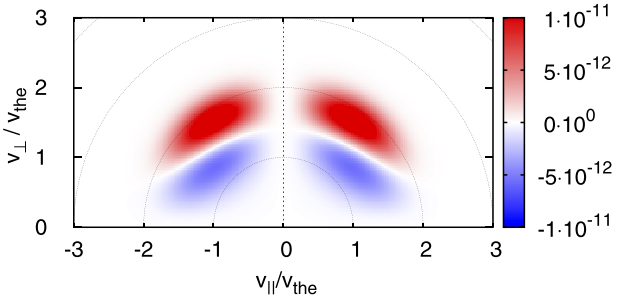

Figure 3. The ECH source term, S^{ECH}. The velocity is normalized by thermal velocity of 1 keV.

the QHS and mirror configurations. There exist finite non-symmetric modes even in the QHS configuration, which is about 2% of the major mode ($n = 4, m = 1$) at $r/a = 0.5$. These non-symmetric modes enhance the radial drift of trapped electrons [15].

The effect of the magnetic configuration in the HSX on the plasma flow have been intensively investigated. Flow measurement experiments have been undertaken using the charge exchange recombination spectroscopy system [10, 16]. The parallel neoclassical viscosity of the QHS configuration is known to be smaller than that of the mirror configuration due to the presence of helical symmetry in the former and not in the latter; thus it can be expected that the parallel flow velocity in the QHS configuration is greater than that observed in the mirror configuration. However, the parallel flow observed in the QHS configuration [11, 14] is smaller than that observed in the mirror configuration.

It has been found that ECH can enhance the radial electron flux due to the radial drift of supra-thermal trapped electrons in heliotron/stellarator plasmas [17]; this electron flux results in a radial current from the supra-thermal electrons, denoted $\mathbf{j}_{\mathrm{se}}$. The net radial current in the steady state should vanish to maintain the quasi-neutrality. Therefore, for the bulk plasma, a return current, $\mathbf{j}_{\mathrm{return}}(= -\mathbf{j}_{\mathrm{se}})$, flows in the steady state by ambipolar condition, and thus the electromagnetic force ($\mathbf{j}_{\mathrm{return}} \times \mathbf{B}$) drives the bulk plasma rotation. We note, moreover, that the supra-thermal electrons drift in the toroidal or helical direction due to the precession motion. During the slowing down of the supra-thermal electrons, they transfer momenta to the bulk plasma via collisions; this momentum transfer is referred to as the collisional force. These forces can be considered to be analogous to the forces by alpha particles

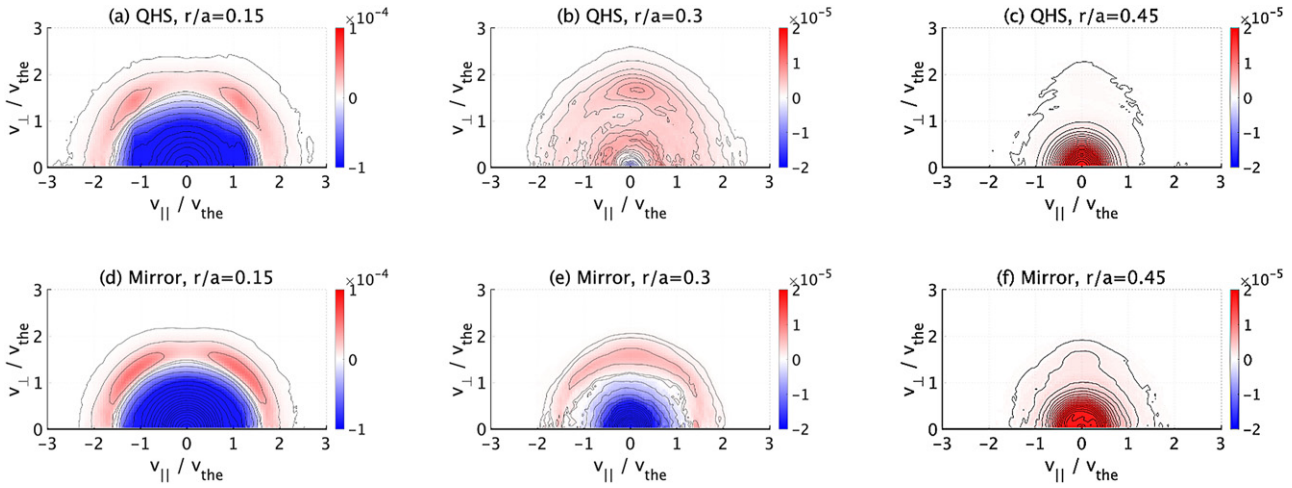

Figure 4. The velocity distribution function, δf with contour lines at several radii in the QHS ((*a*) $r/a = 0.15$, (*b*) 0.3, and (*c*) 0.45) and mirror ((*d*) $r/a = 0.15$, (*e*) 0.3, and (*f*) 0.45) configurations. The velocity is normalized by thermal velocity of 1 keV.

[18–20], neutral beam injection [21], and ion cyclotron resonance heating [22]. We previously reported that ECH can exert forces on the plasma via the $\mathbf{j}_{\text{return}} \times \mathbf{B}$ and collisional forces [15, 23]. The $\mathbf{j}_{\text{return}} \times \mathbf{B}$ forces were also found to dominate over the collisional forces in non-symmetric configurations; in axisymmetric configurations, however, the two forces generated by the heating source without an initial momentum input were found to cancel each other out toroidally [18, 19].

In this work, we evaluate the $\mathbf{j}_{\text{return}} \times \mathbf{B}$ and collisional forces in the HSX. Including the $\mathbf{j}_{\text{return}} \times \mathbf{B}$ forces, which are dominant in both the QHS and mirror configurations, we evaluate the parallel flow driven by the $\mathbf{j}_{\text{return}} \times \mathbf{B}$ force, and we compare them with the flows observed in experiments.

2. Simulation model

To evaluate the $\mathbf{j}_{\text{return}} \times \mathbf{B}$ and collisional forces, we apply the GNET code [17], which can solve a linearized drift kinetic equation for energetic electrons by ECH in five-dimensional phase space via the Monte Carlo method. The drift kinetic equation for the deviation of the electron distribution function from the Maxwell distribution, δf, is given by

$$\frac{\partial \delta f}{\partial t} + (\mathbf{v}_{\text{d}} + \mathbf{v}_{\parallel}) \cdot \frac{\partial \delta f}{\partial \mathbf{r}} + \dot{\mathbf{v}} \cdot \frac{\partial \delta f}{\partial \mathbf{v}} - C(\delta f) - L(\delta f) = S^{\text{ECH}}, \tag{1}$$

where C, L, S^{ECH}, $\mathbf{v}_{\parallel}$, and $\mathbf{v}_{\text{d}}$ are the linear collision operator, the particle sink term, the ECH heating source [24, 25], and the parallel and drift velocities of the electrons, respectively. The GNET code can evaluate the radial current of the supra-thermal electrons induced by ECH, which results in the $\mathbf{j}_{\text{return}} \times \mathbf{B}$ force, and the parallel momenta which the supra-thermal electrons transfer to the bulk plasma, i.e., the collisional force.

In this paper, we use the fluid approach to solve the momentum balance equation [26, 27]. We solve the first-order momentum balance equations multiplied by the magnetic field $\mathbf{B}$ and the poloidal component of the magnetic field $\mathbf{B}_{\text{P}} (\equiv B^{\theta}\mathbf{e}_{\theta})$,

$$m_{\text{i}} N_{\text{i}} \frac{\partial}{\partial t} \langle \mathbf{B} \cdot \mathbf{U}_{\text{i}} \rangle = - \langle \mathbf{B} \cdot \nabla \cdot \boldsymbol{\pi}_{\text{i}} \rangle - m_{\text{i}} N_{\text{i}} \nu_{\text{in}} \langle \mathbf{B} \cdot \mathbf{U}_{\text{i}} \rangle , \tag{2}$$

and

$$m_{\text{i}} N_{\text{i}} \frac{\partial}{\partial t} \langle \mathbf{B}_{\text{P}} \cdot \mathbf{U}_{\text{i}} \rangle = -B^{\theta} B^{\zeta} \langle \mathbf{j}_{\text{return}} \cdot \nabla V \rangle - \langle \mathbf{B}_{\text{P}} \cdot \nabla \cdot \boldsymbol{\pi}_{\text{i}} \rangle - m_{\text{i}} N_{\text{i}} \nu_{\text{in}} \langle \mathbf{B}_{\text{P}} \cdot \mathbf{U}_{\text{i}} \rangle , \tag{3}$$

where $\mathbf{e}_{\theta}$, B^{θ}, B^{ζ}, m_{i}, N_{i}, $\boldsymbol{\pi}_{\text{i}}$, $\boldsymbol{U}_{\text{i}}$, and ν_{in} are the poloidal covariant basis vector, the poloidal and toroidal contravariant components of magnetic field in the Hamada coordinate system, the ion mass, the ion particle density, the viscosity tensor, the ion fluid velocity, and the ion-neutral collision frequency, respectively. We consider the proton-H collision and proton-H^2 collision as the ion-neutral collision. The detailed formulations are described in references [28–30]. The parallel neoclassical viscosity, in its linear form, is given by,

$$\langle \mathbf{B} \cdot \nabla \cdot \boldsymbol{\pi} \rangle = \mu_{\theta} U^{\theta} + \mu_{\zeta} U^{\zeta} \tag{4}$$

$$\langle \mathbf{B}_{\text{P}} \cdot \nabla \cdot \boldsymbol{\pi} \rangle = \mu_{\theta}^{\text{P}} U^{\theta} + \mu_{\zeta}^{\text{P}} U^{\zeta}, \tag{5}$$

where U^{θ} and U^{ζ} are the poloidal and toroidal contravariant components of the flow velocity, respectively. We adopted the analytical expression in the plateau regime for the viscosity coefficients μ_{θ}, μ_{ζ}, μ_{θ}^{P}, and μ_{ζ}^{P} [31, 32].

The first term in the right-hand side of equation (3) corresponds to the $\mathbf{j}_{\text{return}} \times \mathbf{B}$ force, which acts as a driving force. As the $\mathbf{j}_{\text{return}} \times \mathbf{B}$ force is perpendicular to the magnetic field, it does not directly drive the parallel flow. The neoclassical viscosity modifies the flow direction and thus the $\mathbf{j}_{\text{return}} \times \mathbf{B}$ force indirectly drives the parallel flow. The $\mathbf{j}_{\text{return}} \times \mathbf{B}$ force drives the flow until the driving force balances with the damping forces that originate from the neoclassical viscosity and

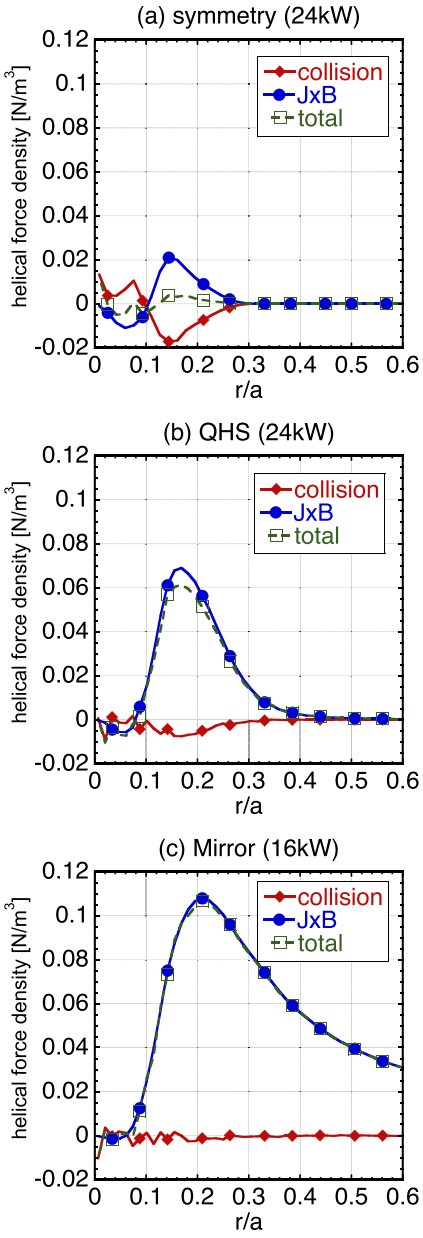

Figure 5. The helical component of the collisional, $\mathbf{j}_{\mathrm{return}} \times \mathbf{B}$ and the total force.

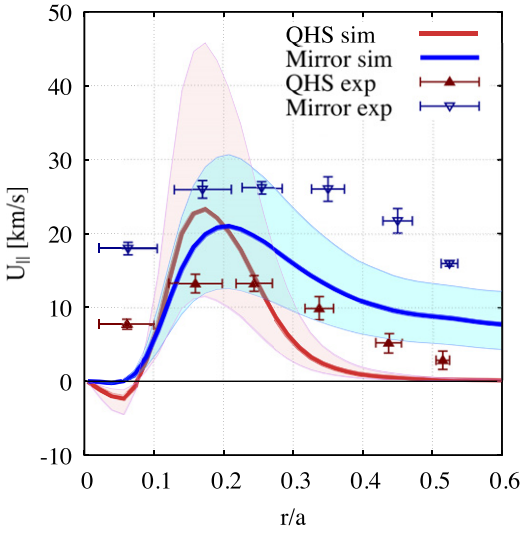

Figure 6. Comparisons of the evaluated and observed parallel flows without the diffusion effect.

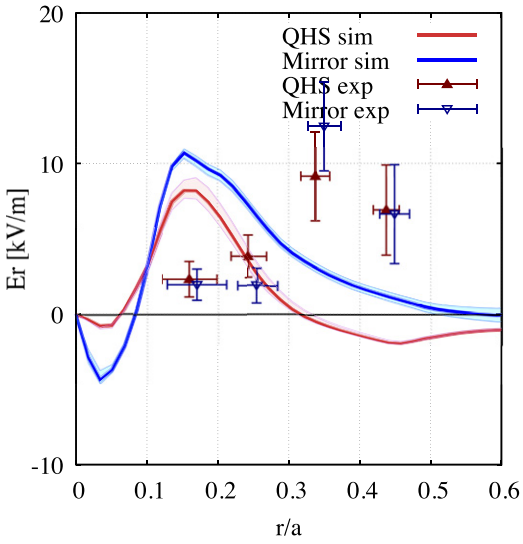

Figure 7. Comparisons of the evaluated and observed radial electric fields without the diffusion effect.

the ion-neutral collisions. The collisional force is not included in the momentum balance equation because it is negligibly small; this is demonstrated in figure 5 and in the existing literature [15].

The return current density $\mathbf{j}_{\mathrm{return}}$, which is driven by the radial electron current density $\mathbf{j}_{\mathrm{se}}$, satisfies Ampère law

$$-\varepsilon_0 \frac{\partial \langle \mathbf{E} \cdot \nabla V \rangle}{\partial t} = \langle \mathbf{j}_{\mathrm{return}} \cdot \nabla V \rangle + \langle \mathbf{j}_{\mathrm{se}} \cdot \nabla V \rangle. \qquad (6)$$

In the steady state, the left-hand side of equation (6) is equal to zero, and thus the return current cancels out exactly the electron current driven by ECH, i.e. $\mathbf{j}_{\mathrm{return}} + \mathbf{j}_{\mathrm{se}} = 0$.

In the neoclassical theory, the perpendicular flow velocity of the lowest order is given by the $E \times B$ flow and the diamagnetic flow, and the parallel flow velocity of the lowest order is given by [10, 32]

$$\mathbf{U}_{\|} = \left(\Phi' + \frac{1}{e_{\mathrm{i}} N_{\mathrm{i}}} p_{\mathrm{i}}' \right) h\mathbf{B} + \lambda_{\mathrm{i}} \mathbf{B}, \qquad (7)$$

where $\lambda_{\mathrm{i}} = \langle \mathbf{U}_{\mathrm{i}} \cdot \mathbf{B} \rangle / \langle B^2 \rangle$ and h is a geometrical factor defined as

$$\mathbf{B} \cdot \nabla h = \frac{2}{B^3} (\mathbf{B} \times \nabla \psi) \cdot \nabla B, \quad \langle hB^2 \rangle = 0, \qquad (8)$$

where ψ is the toroidal flux.

The first term in equation (7) is the return flow or the Pfirsch–Schlüter flow, whose flux-surface average vanishes, and the second term is the mean parallel flow, which is divergence free. From equations (2)–(7), we can obtain a set of simultaneous equations for $\mathrm{d}\lambda_{\mathrm{i}}/\mathrm{d}t$, λ_{i}, $\mathrm{d}\Phi'/\mathrm{d}t$ and Φ'; these detailed formulations can be found in reference [26]. In this

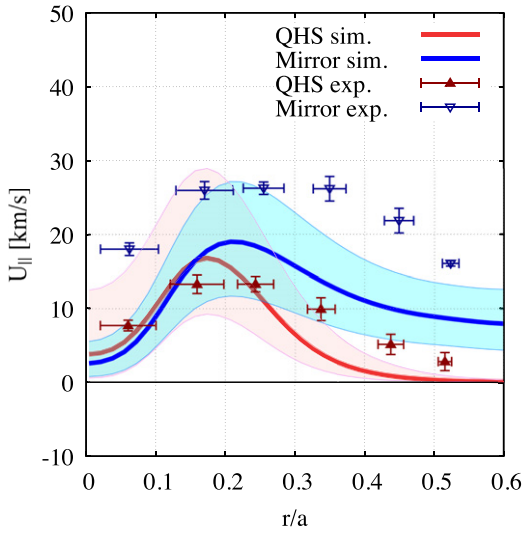

Figure 8. Comparisons of the evaluated and the observed parallel flows including the diffusion effect.

paper, we describe $\lambda_i B_0$ as the mean parallel velocity with the magnetic field at the axis $B_0(= 1\ \mathrm{T})$.

We can evaluate the radial electron current using the GNET code, which takes the radial electric field profile as an input. Solving the momentum balance equation, where the radial electron current is input, we can evaluate the radial electric field and the flow velocity. The radial electron current is affected by the radial electric field, and vice versa. To take these dependences into account, we iterate the calculations using the GNET code and the momentum balance equation until the results converge.

3. Simulation results

We perform simulations using values of temperature and density typical of the HSX experimental conditions. The radial profiles of the density and temperature are shown in figure 2. The QHS configuration shows a higher electron temperature due to the better confinement at the same injected ECH power (100 kW). The ion temperature is low both in the QHS and mirror configurations; it takes a value of approximately 50 eV. The absorbed power, which is evaluated by the ray-tracing code, is 24 kW in the QHS configuration and 16 kW in the mirror configuration. The ECH heating location locates around $r/a \approx 0.1$.

Using the GNET code, we evaluate the velocity space distribution of the supra-thermal electrons by ECH, and estimate the $\mathbf{j}_r \times \mathbf{B}$ and collisional forces in the HSX. The example of the O-mode ECH quasi-linear heating term in the velocity space is shown in figure 3, and the obtained velocity distributions δf at three minor radii are shown in figure 4. The positive (negative) δf means increase (decrease) of the distribution function from Maxwellian. The peaks of positive δf around the heating location ($r/a = 0.15$) are at $(v_\parallel/v_{\mathrm{the}}, v_\perp/v_{\mathrm{the}}) = (\pm 1.2, 1.2)$ both in the QHS and mirror configurations. These peaks are generated by the ECH heating source. However, the peaks of δf at $r/a = 0.3$, where is apart from the heating location, are at $v_\parallel = 0$ due to the orbit effect of trapped electrons. The radial diffusion of supra-thermal electrons are generated by the radial drift of trapped electrons. The radial electron drift is large in the mirror configuration, so the supra-thermal electron distribution are radially broader than that in the QHS configuration. The supra-thermal electrons move radially, and then get thermalized as shown in figures 4(e) and (f).

The force in the symmetry ($n = 4, m = 1$) direction of the HSX is shown in figure 5. The component of the force in the symmetry direction is important because the plasma tends to flow primarily in the direction of helical symmetry due to the neoclassical viscosity; the plasma flow perpendicular to the symmetric direction is strongly damped [16, 27, 33]. In the case of a completely helically symmetric configuration with only the ($n = 4, m = 1$) mode, the $\mathbf{j}_{\mathrm{return}} \times \mathbf{B}$ and collisional forces roughly cancel each other out, and thus the total force (given by the summation of the $\mathbf{j}_{\mathrm{return}} \times \mathbf{B}$ and collisional forces) is small. In this case, the conservation of angular momentum is satisfied, and the total force in the symmetry direction approaches zero, except for the force due to the finite orbit effect. However, non-symmetric magnetic modes enhance the radial diffusion of electrons. Even in the QHS configuration, whose non-symmetric modes are small, the $\mathbf{j}_{\mathrm{return}} \times \mathbf{B}$ force is dominant, and there is a nonzero total force in the symmetry direction; this nonzero total force in the symmetry direction is due to small non-symmetric modes. The peak value of the total force in the mirror configuration is about twice as large as that obtained in the QHS configuration despite the lower absorbed power in the mirror configuration. The collisional force is sufficiently small to be neglected in the flow calculations in the QHS and mirror configurations.

Here, we evaluate the parallel flow expected in the experimental conditions. Figure 6 shows the calculated and observed flow velocity profiles in the QHS and mirror configurations. The neutral damping is also an important factor in evaluations of the plasma flow [14], and the hatched regions in figure 6 correspond to the uncertainty regarding the neutral density. The reference value of the neutral density is calculated using the DEGAS code [34]. The upper limit of the neutral density is equal to twice that obtained using the DEGAS code, and the lower limit is half of the DEGAS result. The obtained flow in the QHS configuration shows a clear peak around the ECH heating location because the radial electron current is localized due to the small radial diffusion of supra-thermal electrons. The parallel flow in the mirror configuration is greater than that obtained in QHS configuration with the exception of that obtained in the region close to the peak.

The obtained radial electric field is shown in figure 7. The hatched regions correspond to the uncertainty of the neutral densities as figure 6. The predicted peak in the value of E_r is located at $r/a \approx 0.15$, just beside the ECH heating location; the peak in the observed values of E_r is located at $r/a \approx 0.3$. The difference may be due to the use of the linear model of viscosity; the linear model is not able to capture the effect of poloidal resonances. Although the peak value of E_r obtained via simulations is slightly shifted inward, the maximum values of E_r obtained via simulations and experiments are comparable. While the neutral damping has a significant effect on the

flow velocity, the radial electric field does not change because the plasma radial conductivity is only weakly dependent on the neutral damping rate.

In the above calculations, the radial interaction, i.e., the perpendicular viscosity, is ignored, and the equations are based on the assumption that the radial momentum flux is small. However, there may exist a nonnegligible quantity of the radial diffusion of momentum in the QHS configuration with such a steep velocity gradient. We introduce the diffusion effect in equations (2) and (3) artificially as a small correction. Here, as a boundary condition, we set the flow velocity at $r/a = 1$ to be zero. The results obtained for a diffusion coefficient $D = 0.025(\mathrm{m}^2\,\mathrm{s}^{-1})$ are shown in figure 8. The steep gradient in the QHS configuration is seen to be smoothened as a result of the addition of the diffusion effect, and the simulation results show a closer agreement with the experimental findings.

4. Conclusions

In order to investigate the mechanism behind the parallel flow induced by ECH in the HSX, using the GNET code, we have calculated the $\mathbf{j}_{\mathrm{return}} \times \mathbf{B}$ and collisional forces that arise as a result of ECH. Even in the QHS configuration, the $\mathbf{j}_{\mathrm{return}} \times \mathbf{B}$ force is dominant over the collisional forces, and there is a nonzero total force in the symmetry direction due to small non-symmetric modes. The peak value of the force in the mirror configuration is almost twice as large as that obtained in the QHS configuration despite the lower quantity of absorbed power.

Experimentally, the plasma tends to flow in the symmetry direction due to the neoclassical viscosity, and the neutral damping is an important factor in the plasma flow. Solving the momentum balance equations including the contributions from the $\mathbf{j}_{\mathrm{return}} \times \mathbf{B}$ force, the neoclassical viscosity, and the neutral damping, we evaluated the parallel flow velocities. The calculated flow in the mirror configuration is larger than that obtained in the QHS configuration despite the larger neoclassical viscosity and the lower absorption power. We have obtained reasonable agreement between the results of simulation and experiment, and found that the $\mathbf{j}_{\mathrm{return}} \times \mathbf{B}$ force driven by ECH plays a crucial role in the HSX.

Acknowledgments

The authors would like to thank the HSX group for providing data and fruitful discussions. This work is supported by a Grant-in-Aid for Scientific Research (C), No. 18K03582, JSPS Core-to-Core Program, A. Advanced Research Networks (PLADyS) and Japan/U.S. Cooperation in Fusion Research and Development. This work was carried out using the Plasma Simulator (FUJITSU FX100) of NIFS and JFRS-1 supercomputer system at IFERC-CSC.

ORCID iDs

Y. Yamamoto https://orcid.org/0000-0002-2197-1506
S. Murakami https://orcid.org/0000-0002-2526-7137
S.T.A. Kumar https://orcid.org/0000-0002-6444-5178

References

[1] Lin Z., Hahm T.S., Lee W.W., Tang W.M. and White R.B. 1998 *Science* **281** 1835
[2] Terry P.W. 2000 *Rev. Mod. Phys.* **72** 109
[3] Chu M.S. and Okabayashi M. 2010 *Plasma Phys. Control. Fusion* **52** 123001
[4] Strait E.J., Taylor T.S., Turnbull A.D., Ferron J.R., Lao L.L., Rice B., Sauter O., Thompson S.J. and Wróblewski D. 1995 *Phys. Rev. Lett.* **74** 2483
[5] Bondeson A. and Ward D.J. 1994 *Phys. Rev. Lett.* **72** 2709
[6] Rice J.E. *et al* 2007 *Nucl. Fusion* **47** 1618
[7] Rice J.E. 2008 *J. Phys.: Conf. Ser.* **123** 012003
[8] Angioni C. *et al* (ASDEX Upgrade Team) 2011 *Phys. Rev. Lett.* **107** 215003
[9] Yoshida M., Kamada Y., Takenaga H., Sakamoto Y., Oyama N. and Urano H. (the JT-60 Team) 2009 *Nucl. Fusion* **49** 115028
[10] Kumar S.T.A., Talmadge J.N., Dobbins T.J., Anderson F.S.B., Likin K.M. and Anderson D.T. 2017 *Nucl. Fusion* **57** 036030
[11] Kumar S.T.A., Dobbins T.J., Talmadge J.N., Wilcox R.S. and Anderson D.T. 2018 *Plasma Phys. Control. Fusion* **60** 054012
[12] Callen J.D., Cole A.J. and Hegna C.C. 2009 *Nucl. Fusion* **49** 085021
[13] Idomura Y. 2017 *Phys. Plasmas* **24** 080701
[14] Dobbins T.J., Kumar S.T.A., Talmadge J.N. and Anderson D.T. 2019 *Nucl. Fusion* **59** 046007
[15] Yamamoto Y., Murakami S., Chang C.-C., Kumar S.T.A., Talmadge J.N., Likin K. and Anderson D.T. 2019 *Plasma Fusion Res.* **14** 3403105
[16] Briesemeister A., Zhai K., Anderson D.T., Anderson F.S.B., Lore J. and Talmadge J.N. 2010 *Contrib. Plasma Phys.* **50** 741
[17] Murakami S., Gasparino U., Idei H., Kubo S., Maassberg H., Marushchenko N., Nakajima N., Romé M. and Okamoto M. 2000 *Nucl. Fusion* **40** 693
[18] Rosenbluth M.N. and Hinton F.L. 1996 *Nucl. Fusion* **36** 55
[19] Snicker A., Asunta O., Ylitie H., Kurki-Suonio T., Schneider M. and Pinches S.D. 2015 *Nucl. Fusion* **55** 063023
[20] Honda M., Takizuka T., Tobita K., Matsunaga G. and Fukuyama A. 2011 *Nucl. Fusion* **51** 073018
[21] Honda M., Takizuka T., Fukuyama A., Yoshida M. and Ozeki T. 2009 *Nucl. Fusion* **49** 035009
[22] Chan V.S., Chiu S.C. and Omelchenko Y.A. 2002 *Phys. Plasmas* **9** 501
[23] Yamamoto Y., Murakami S., Chang C.C., Takahashi H., Ida K., Yoshinuma M. and Ko W.H. 2021 *Phys. Plasmas* **28** 102501
[24] Romé M., Erckmann V., Gasparino U., Hartfuß H.J., Kühner G., Maaßberg H. and Marushchenko N. 1997 *Plasma Phys. Control. Fusion* **39** 117
[25] Hasegawa S., Murakami S. and Moriya Y. 2013 *Plasma Fusion Res.* **8** 2403083
[26] Coronado M. and Talmadge J.N. 1993 *Phys. Fluids* B **5** 1200
[27] Gerhardt S.P., Talmadge J.N., Canik J.M. and Anderson D.T. 2005 *Phys. Plasmas* **12** 056116

[28] Gerhardt S.P. 2004 Measurements and modeling of the plasma response to electrode biasing in the HSX stellarator *PhD Thesis* University of Wisconsin-Madison
[29] Krstić P.S. and Schultz D.R. 1999 *Atomic and Plasma–Material Interaction Data for Fusion* (Vienna: IAEA) **8** 1
[30] Tabata T. and Shirai T. 2000 *At. Data Nucl. Data Tables* **76** 1
[31] Shaing K.C., Hirshman S.P. and Callen J.D. 1986 *Phys. Fluids* **29** 521
[32] Coronado M. and Wobig H. 1986 *Phys. Fluids* **29** 527
[33] Spong D.A. 2005 *Phys. Plasmas* **12** 056114
[34] Heifetz D., Post D., Petravic M., Weisheit J. and Bateman G. 1982 *J. Comput. Phys.* **46** 309